627

An analytical model for shear links
in eccentrically braced frames

Amir Ashtari [1] and Saeed Erfani [*2]

[1] *Department of Civil Engineering, Science and Research Branch, Islamic Azad University, Tehran, Iran*
[2] *Department of Civil Engineering, Amirkabir University of Technology, Tehran, Iran*

Abstract. When an eccentrically braced frame (EBF) is subjected to severe earthquakes, the links experience inelastic deformations while beams outside of the link, braces and columns are designed to remain elastic. To perform reliable inelastic analyses of EBFs sufficient analytical model which can accurately predict the inelastic performance of the links is needed. It is said in the literature that available analytical models for shear links generally predict very well the maximum shear forces and deformations from experiments on shear links, but may underestimate the intermediary values. In this study it is shown that available analytical models do not predict very well the maximum shear forces and deformations too. In this study an analytical model which can accurately predict both maximum and intermediary values of shear force and deformation is proposed. The model parameters are established based on test results from several experiments on shear links. Comparison of available test results with the hysteresis curves obtained using the proposed analytical model established the accuracy of the model. The proposed model is recommended to be used to perform inelastic analyses of EBFs.

Keywords: eccentrically braced frame; shear link; analytical model; inelastic analysis; hysteresis curves

1. Introduction

Eccentrically braced frames (EBF) offer high lateral stiffness because of their braced configuration while also providing high ductility and energy dissipation (Kanvinde *et al*. 2014). They are widely used as a lateral-force resisting system for multi-story buildings located in seismic areas (Wang *et al*. 2016). The key components of the EBF system include columns, collector beams, braces and active links. The active links are designed to provide ductility and energy dissipation through yielding under design basis earthquakes, while all other structural members are designed to be stronger than the links and stay in elastic range (Xu *et al*. 2016). The distinguishing characteristic of an EBF is that at least one end of every brace is connected so that the brace force is transmitted through shear and bending of a short beam segment, called the link. The link is defined by a horizontal eccentricity between the intersection points of the two brace centerlines with the beam centerline (or between the intersection points of the brace and column centerlines

---

with the beam centerline for links adjacent to columns) (AISC 341 2010).

The link length, e, is often normalized with respect to the ratio between the plastic moment capacity, M_P, and the plastic shear capacity, V_P, of the link section. This normalized link length, ρ, is called the length ratio. Links with a length ratio less than 1.6, called short or shear links, yield primarily in shear and can be designed for 0.08 radian inelastic rotation (γ). Links with length ratio greater than 2.6, called long links, form flexural hinges at either end and can be designed for 0.02 radian inelastic rotation. Links with length ratios between 1.6 and 2.6, called intermediate links, experience a combination of flexural and shear yielding and can be designed for inelastic rotations between 0.02 and 0.08 radian depending on the length ratio (Richards and Uang 2005). The link member should have enough energy dissipation capacity before ductile failure to prevent collapse of the frame (Ohsaki and Nakajima 2012). The EBFs are most commonly designed using shear-yielding links (Okazaki *et al.* 2014). Shear links are always advisable since they showed better ductility, stiffness and strength (Daneshmand and Hosseini Hashemi 2012). By selecting relatively short links the EBF systems tend to be relatively stiff, which is advantageous for the control of serviceability drift limits (O'Reilly and Sullivan 2013). Lian *et al.* (2015) investigated EBFs with high strength steel combination to reduce steel consumption and increase economic efficiency. Montuori *et al.* (2015) developed a design procedure, based on the Theory of Plastic Mechanism Control (TPMC), by means of Incremental Dynamic Analyses (IDA) pointing out the fulfilment of the design goal. O'Reilly and Sullivan (2016) developed a set of fragility functions for EBF structures, considering that damage can be directly linked to the interstorey drift demand at each storey.

Analytical models that are used to study the inelastic seismic response of the EBFs usually reflect the anticipated behavior of the different frame elements. Links are modeled as inelastic elements with concentrated end flexural and shear hinges. Beams outside of the link, braces, and columns are typically modeled as elastic beam-column elements, because no inelastic behavior is anticipated in design (Koboevic *et al.* 2012).

Ricles and Popov (1994) proposed an analytical model for shear links. It is based on the single-component model and consists of a linear elastic beam with nonlinear hinges at each end. Each hinge is of zero length, and is consisted of a series of three sub-hinges in which plastic deformations are concentrated. Inelastic response of each link is described by a multilinear function. Ramadan and Ghobarah (1995) replaced the sub-hinges with translational and rotational springs and proposed a new model. Both models had incorrect shear stiffness so that the shear stiffness of model was half the link shear stiffness. Richards and Uang (2006) corrected the shear stiffness of the model proposed by Ramadan and Ghobarah (1995), and proposed a new analytical model for shear links. Koboevic *et al.* (2012) claimed that these analytical models predict very well the maximum shear forces and deformations but underestimate the intermediary values. They proposed an analytical model based on the results of experimental test performed by Okazaki and Engelhardt (2007), regardless of the fact that the actual measured dimensions of sections were different from the standard dimensions of sections. To account for this difference between the actual and standard dimensions of sections, despite of what is said in their paper, the strain-hardening ratio is set to 0.0045. For this reason, the shear stiffness of their proposed model is incorrect and the predicted shear forces are 15 to 24 percent more than the experimental shear forces. To study the behavior of the link alone, maximum shear forces and deformations may be enough but for proper analysis of the whole EBF, intermediary values are needed too. In this study it is shown that available analytical models do not predict very well the maximum shear forces and deformations too. In this study an analytical model which can accurately predict both maximum

and intermediary values of shear force and deformation is proposed. The OpenSees program is used to construct numerical models. The model parameters were determined by calibration against data from 11 cyclic tests on shear links by Okazaki and Engelhardt (2007). Then the proposed model is verified by comparing the predicted shear forces and deformations with the test results of 7 cyclic tests on shear links by Kasai and Popov (1986) and 1 cyclic test on a large scale 1-story EBF by Berman and Bruneau (2007). Comparison of available test results with the hysteresis curves obtained using the proposed analytical model established the accuracy of the model. To compare the numerical results of the available analytical models and the proposed analytical model, nonlinear dynamic analysis of a four-story EBF subjected to El Centro earthquake was performed. The proposed model is recommended to be used to perform inelastic analyses of EBFs.

2. Proposed Analytical Model

2.1 Element description

The development of a simple analytical model which can accurately predict the response of shear links, is attempted. The OpenSees program is used to construct numerical models. The proposed element is defined by four nodes and is consisted of an elastic beam-column element and two zero-length shear springs. As shown in Fig. 1, i and j are the inner nodes and, $i^{'}$ and $j^{'}$ are the outer nodes. The elastic beam-column element connects the two inner nodes. The outer
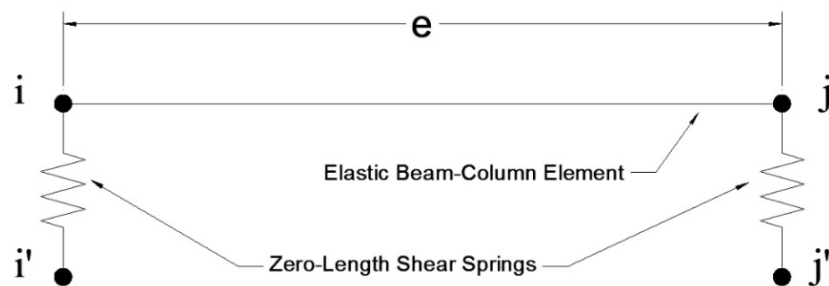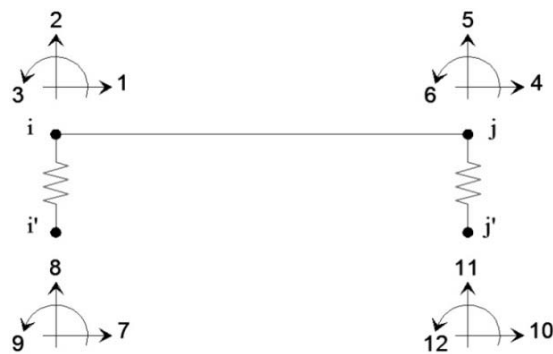

Fig. 1 Shear link model

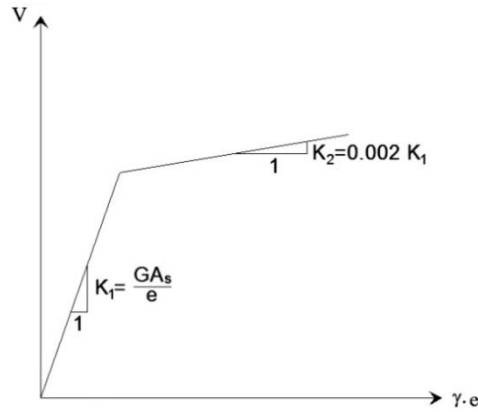Fig. 2 Degrees of freedom for shear link model

Fig. 3 Bilinear link shear force-deformation response

nodes have the same coordinates as the inner nodes and are used to define zero-length shear springs. The elastic beam-column element is constrained to perform elastically under any loading condition without yielding or the formation of plastic hinges at its ends. The length of this element (i.e., the distance between node *i* and *j*) is taken equal to the link length, *e*.

The degrees of freedom (DOFs) of the inner and outer nodes are shown in Fig. 2. The inner and outer nodes are constrained so that the DOFs 1, 3, 4, and 6 are equal to the DOFs 7, 9, 10, and 12, respectively. The DOFs 2 and 5 are connected by zero-length shear springs to the DOFs 8 and 11, respectively.

In the current study, properties of the shear springs were determined by calibration against data from 11 cyclic tests on shear links by Okazaki and Engelhardt (2007). Then the proposed model is verified by comparing the predicted shear forces and deformations with the test results of 7 cyclic tests on shear links by Kasai and Popov (1986) and 1 cyclic test on a large scale 1-story EBF by Berman and Bruneau (2007). The obtained bilinear link shear force-deformation relationship is illustrated in Fig. 3.

In Fig. 3, K_1 is the elastic stiffness of the link, K_2 is the post-yield stiffness of the link, G is the shear modulus of elasticity, A_s is the area of the link section considered to resist shear, *e* is the length of link.

The inelastic behavior of the shear springs was described using Giuffré-Menegotto-Pinto (Steel02) hysteretic material. The following Steel02 parameters were determined from calibration against the test data: $F_y = 1.3 R_y V_n$, $E0 = K_s$, $b = \alpha_s$, $R_0 = 17.0$, $CR1 = 0.915$, $CR2 = 0.05$, $a_1 = a_3 = 0.0$, $a_2 = a_4 = 1.0$, and *sigInit* $= 0.0$. Where F_y is the yield strength of link material, R_y is the ratio of the expected yield stress to the specified minimum yield stress, V_n is the link nominal shear strength, $E0$ is the initial elastic tangent, K_s is the elastic stiffness of the shear springs, and α_s is strain-hardening ratio (ratio between post-yield tangent and initial elastic tangent) of shear springs, R_0, $CR1$, and $CR2$ are parameters to control the transition between elastic to plastic branches. a_1 is increase of compression yield envelope as proportion of yield strength after a plastic strain of

$a_2 \dfrac{F_y}{E0}$, a_2 is isotropic hardening parameter a_3 is increase of tension yield envelope as proportion

of yield strength after a plastic strain of $a_4 \dfrac{F_y}{E0}$, and a_4 is isotropic hardening parameter. The

values of K_s and α_s should be determined so that the elastic stiffness of the element is equal to K_1 and its post-yield stiffness is equal to K_2. To determine these parameters trial and error approach was used. The value of F_y was obtained so that the maximum shear forces obtained from the numerical results were equal to those obtained from the experimental results. The default values were used for a_1, a_2, a_3, a_4, and *sigInit*. The values of R_0, *CR*1, and *CR*2 were obtained so that the intermediary values of shear force obtained from the numerical results were equal to those obtained from the experimental results.

2.2 Calculation of K_s

The structural properties of the proposed shear link are a combination of elastic beam-column element properties and shear springs properties. The elastic beam-column element and two shear springs are connected in series. The elastic stiffness of the link element is defined

$$K_e = \frac{1}{\dfrac{1}{K_s} + \dfrac{1}{K_{bc}} + \dfrac{1}{K_s}} = \frac{K_s K_{bc}}{K_s + 2K_{bc}} \tag{1}$$

Where K_e is the elastic stiffness of the link element (see Fig. 3), K_s is the elastic stiffness of the shear springs, and K_{bc} is the elastic stiffness of the elastic beam-column element. Setting K_e equal to K_1, there are two evident choices for stiffness of shear hinges:

(a) $K_{bc} = \infty$: in which case $K_s = 2K_1$
(b) $K_s = \infty$: in which case $K_{bc} = K_1$

Both options are not desirable in the context of computer analysis because an infinite stiffness of the elastic beam-column element leads to numerical divergence and an infinite elastic stiffness of the shear springs makes it impossible to express the post-yield stiffness as a fraction of the elastic stiffness. In order to avoid these problems elastic stiffness of the shear springs is taken $2n$ times larger than the stiffness of the elastic beam-column element

$$K_s = 2nK_{bc} \tag{2}$$

Ibarra and Krawinkler (2005) suggested 10 for the value of n. Now the elastic stiffness of the shear springs and the elastic beam-column element is expressed as a function of the link shear stiffness and the multiplier n as

$$K_{bc} = \frac{n+1}{n}K_1 \tag{3}$$

$$K_s = 2(n+1)K_1 \tag{4}$$

Setting n equal to 10, K_{bc} and K_s are defined as

$$K_{bc} = 1.1K_1 \tag{5}$$

$$K_s = 22K_1 \tag{6}$$

2.3 Calculation of α_S

The elastic beam-column element remains elastic during the entire cycles of loading and nonlinear response is entirely due to the shear springs. Because the elastic beam-column element and the shear springs are connected in series, the increment in the deformation of the total element in the post-yielding range is the sum of the increments in deformation of the three sub-elements in this interval

$$\Delta\delta_{Link} = \frac{\Delta V_{in}}{K_{s,s}} + \frac{\Delta V_{in}}{K_{bc}} + \frac{\Delta V_{in}}{K_{s,s}} \tag{7}$$

Where ΔV_{in} is the increment in shear force developed in the inelastic range, $K_{s,s}$ is the stiffness of the shear springs for the strain hardening branch. According to Fig. 3 the increment in the deformation of the link due to ΔV_{in} is defined as

$$\Delta\delta_{Link} = \frac{\Delta V_{in}}{\alpha_L K_1} \tag{8}$$

Where $\alpha_L = \dfrac{K_2}{K_1}$. Setting Eq. (7) equal to Eq. (8) leads to

$$\frac{\Delta V_{in}}{\alpha_L K_1} = \frac{2\Delta V_{in}}{\alpha_s K_s} + \frac{\Delta V_{in}}{K_{bc}} \tag{9}$$

Where $\alpha_s = \dfrac{K_{s,s}}{K_s}$. Substituting Eqs. (3)-(4) in Eq. (9) yields the equation for α_S

$$\frac{1}{\alpha_L} = \frac{1}{\alpha_s(n+1)} + \frac{n}{n+1} \tag{10}$$

Simplifying Eq. (10) leads to

$$\alpha_s = \frac{\alpha_L}{1 + n(1 - \alpha_L)} \tag{11}$$

3. Numerical simulation and verification

3.1 Case 1

Okazaki and Engelhardt (2007) tested 11 shear links with one end attached to a column. Four different wide-flange shapes were used to construct the test specimens. All sections were of ASTM A992 steel. The measured dimensions of sections were different from the standard dimensions of sections. Full details and dimensions of the test setup are shown in Fig. 4.

Four different cyclic loading protocols, as shown in Fig. 5, were used in the tests. As indicated in the figure, the four protocols are referred to as the old-AISC, severe, revised, and random loading protocols. Each loading protocol controls the link rotation angle, γ, which is computed as the relative displacement of one end of the link compared to the other, divided by the link length.
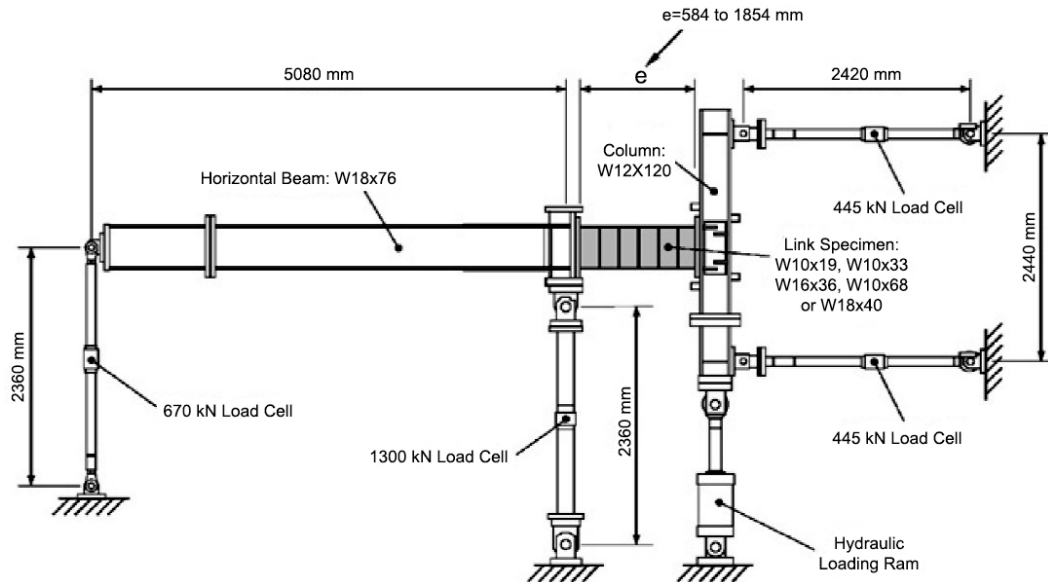
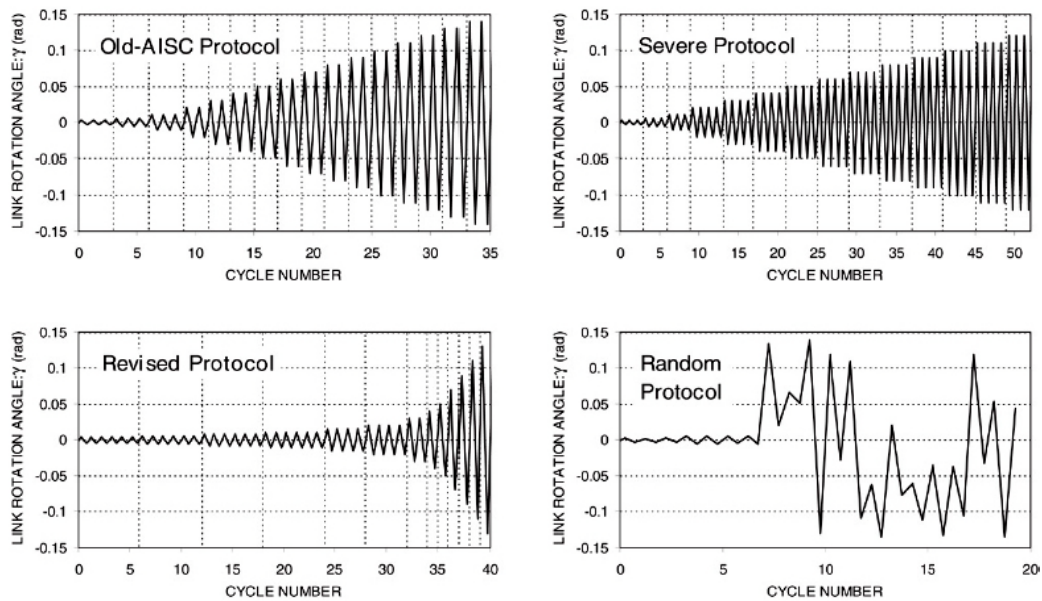Fig. 4 Details and dimensions of test setup (Okazaki and Engelhardt 2007)

Fig. 5 Loading protocols (Okazaki and Engelhardt 2007)

After several initial elastic cycles, the old-AISC loading protocol (Old) requires increasing the applied link rotation in increments of 0.01 rad, with two cycles of loading applied at each increment of rotation. The severe loading protocol (SEV) was identical to the old-AISC protocol, except that four cycles of loading, instead of two cycles, were required at each increment of rotation. The Revised Loading Protocol (RLP) requires that, after completing the loading cycle at a

Table 1 Test Specimens (Okazaki and Engelhardt 2007)

Specimen	Link section	Link length (e)	$e/(M_p/V_p)$	Loading protocol
4A	W10×33	584 mm	1.04	Old
4B	W10×33	584 mm	1.04	Old
4C	W10×33	584 mm	1.04	Old
4A-RLP	W10×33	584 mm	1.04	RLP
4C-RLP	W10×33	584 mm	1.04	RLP
S1	W10×33	584 mm	1.01	SEV
S2	W10×33	584 mm	0.99	SEV
S3	W10×33	584 mm	0.99	SEV
S4	W10×33	584 mm	0.99	SEV
S5	W10×33	584 mm	0.99	SEV
S6	W10×33	584 mm	0.99	SEV
S7	W10×33	584 mm	0.99	SEV
S8	W10×33	584 mm	0.99	RLP
S9	W10×33	584 mm	0.99	RLP
S10	W10×33	584 mm	0.99	RLP
10	W10×68	930 mm	1.25	Old
10-RLP	W10×68	930 mm	1.25	RLP
8	W16×36	930 mm	1.49	Old
8-RLP	W16×36	930 mm	1.49	RLP
12	W18×40	584 mm	1.02	Old
12-RLP	W18×40	584 mm	1.02	RLP
12-SEV	W18×40	584 mm	1.02	SEV
12-RAN	W18×40	584 mm	1.02	RAN

link rotation of 0.05 rad, the link rotation be increased in increments of 0.02 rad, with one cycle of loading applied at each increment of rotation. Finally, the random loading protocol (RAN) was a randomly generated sequence which imposes large rotations in both loading directions during early loading cycles. The old-AISC protocol was specified in the previous, 2002 AISC Seismic Provisions as the loading protocol for testing EBF links.

Table 1 provides a listing of all link test specimens and their loading protocol. The only difference between the specimens with the same link sections and different names, is in their stiffener detailing. The OpenSees model for specimens 4A and 4A-RLP is shown in Fig. 6. The elastic beam-column element was used to model beam and column. Because the measured dimensions of sections are different from the standard dimensions of sections, the stiffness of the OpenSees models should be modified to be the same as the stiffness of the corresponding test specimen.

The numerical result for specimens 4A and 4A-RLP are compared to the experimental result in Figs. 7-8, respectively. As shown in Figs. 7-8 the numerical results fit very well the experimental results and the proposed model not only predicted very well the maximum values of shear force and deformation, but also predicted very well the intermediary values.
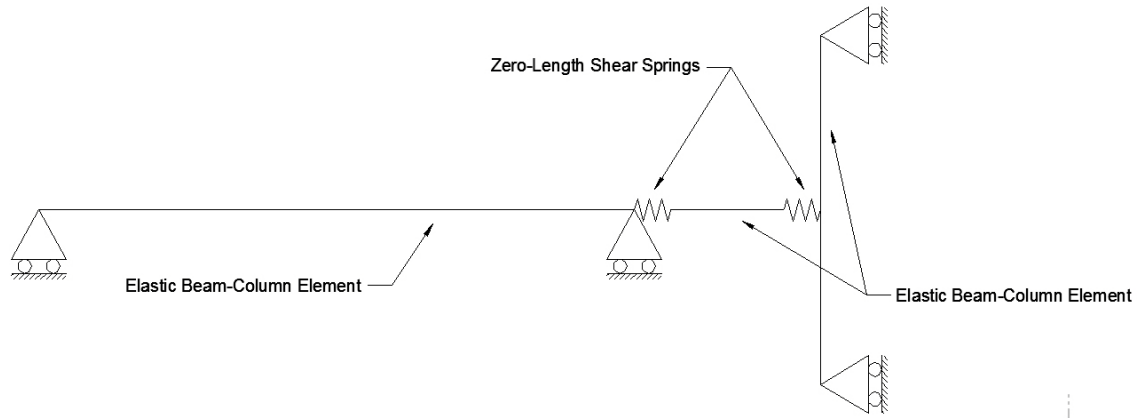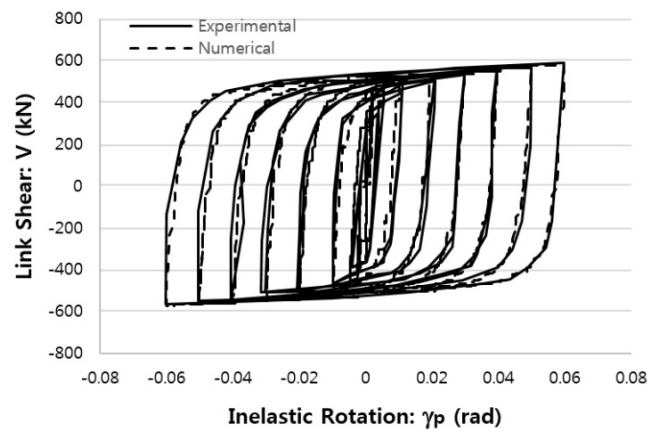
Fig. 6 OpenSees model for specimens 4A and 4A-RLP

Fig. 7 Comparison of experimental and analytical link shear versus link rotation hysteresis curves for specimen 4A using the proposed model
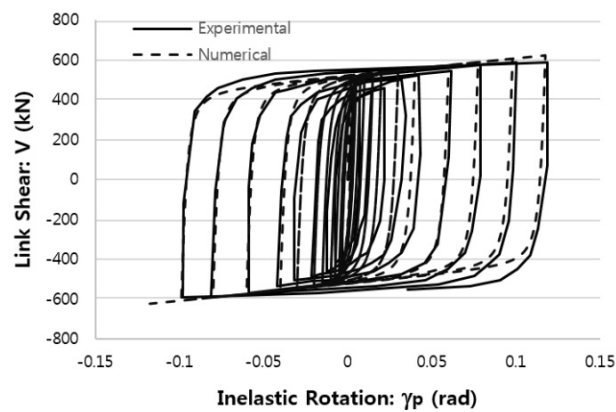

Fig. 8 Comparison of experimental and analytical link shear versus link rotation hysteresis curves for specimen 4A-RLP using the proposed model
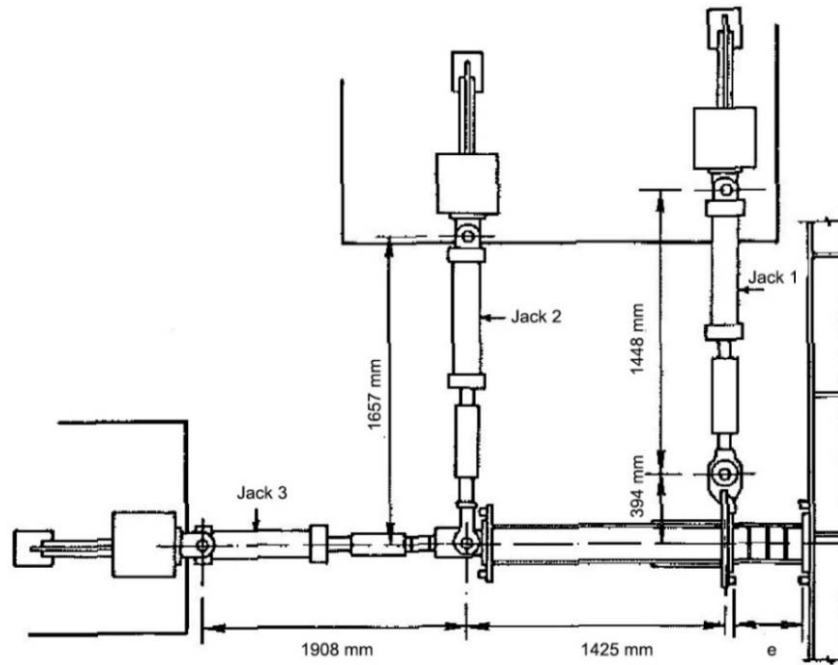
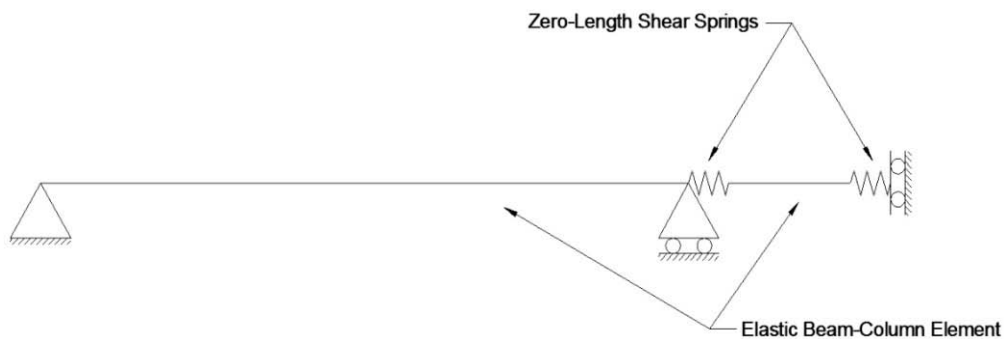Fig. 9 Experimental setup (Kasai and Popov 1986)

Fig. 10 OpenSees model for test setup

3.2 Case 2

Kasai and Popov (1986) tested 7 shear links with one end attached to a column. All link specimens were of W8×10 sections. All specimens were made of ASTM A36 steel. The test setup is shown in Fig. 9. The OpenSees model for specimens 5 and 7 is shown in Fig. 10.

As indicated in Table 2, the applied loadings were varied for different specimens: monotonically increasing displacement was applied to Specimen 1, and cyclic displacements were applied to all other specimens. The cyclic displacement history consisted of one cycle at $\delta = \pm 0.25$ in. (6.35 mm) and two cycles at $\delta = \pm 0.5$ in. (12.7 mm), ± 0.75 in. (19.05 mm), ± 1.0 in. (25.4 mm) ..., until failure of the specimen occurred.

The numerical result for specimens 5 and 7 are compared to the experimental result in Figs. 11-12, respectively. As shown in Figs. 11-12 the numerical results fit very well the experimental results and the proposed model not only predicted very well the maximum values of shear force and deformation, but also predicted very well the intermediary values.

Table 2 Test specimens (Kasai and Popov 1986)

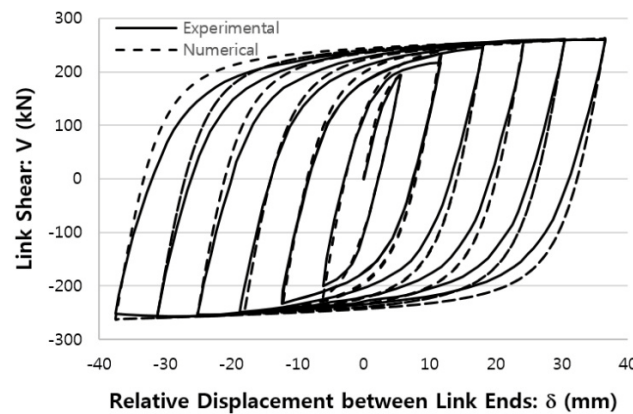| Specimen number	e (mm)	Loading
1	368.3	Monotonic (twice)
2	368.3	Cyclic
3	368.3	Cyclic
4	368.3	Cyclic + Axial force
5	444.5	Cyclic
6	444.5	Cyclic + Axial force
7	444.5	Cyclic

Fig. 11 Comparison of experimental and analytical link shear versus relative displacement between link ends hysteresis curves for specimen 5 using the proposed model
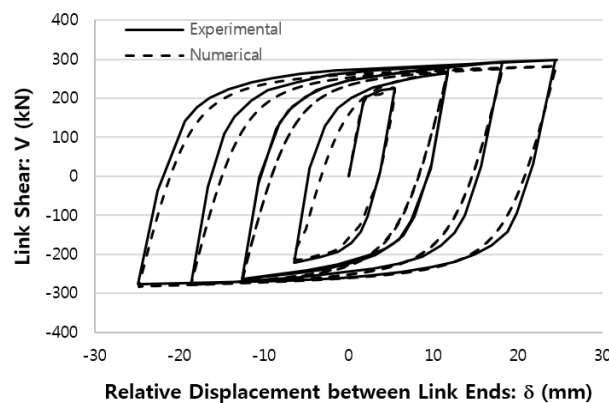

Fig. 12 Comparison of experimental and analytical link shear versus relative displacement between link ends hysteresis curves for specimen 7 using the proposed model
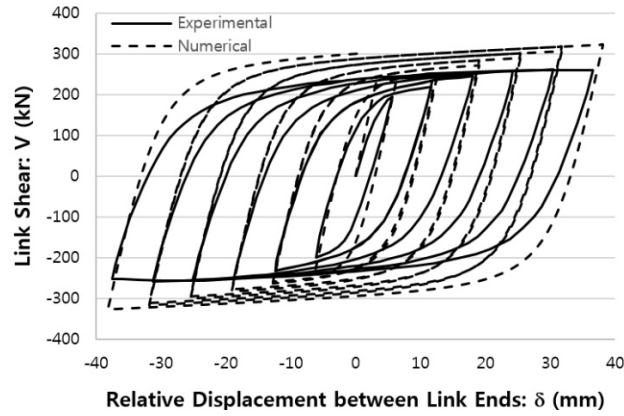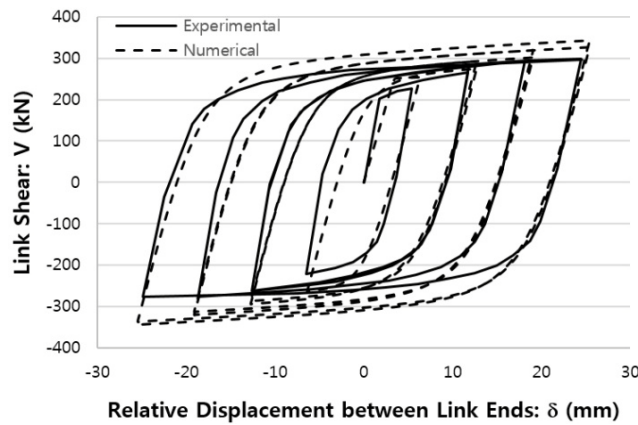
Fig. 13 Comparison of experimental and analytical link shear versus relative displacement between link ends hysteresis curves for specimen 5 using the proposed model by Koboevic *et al*. (2012)

Fig. 14 Comparison of experimental and analytical link shear versus relative displacement between link ends hysteresis curves for specimen 7 using the proposed model by Koboevic *et al*. (2012)
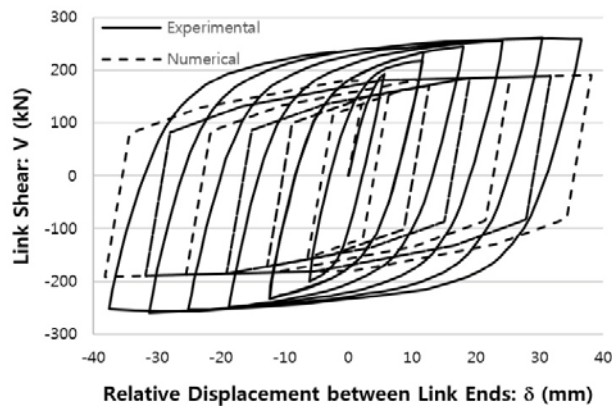

Fig. 15 Comparison of experimental and analytical link shear versus relative displacement between link ends hysteresis curves for specimen 5 using the proposed model by Richards and Uang (2005)
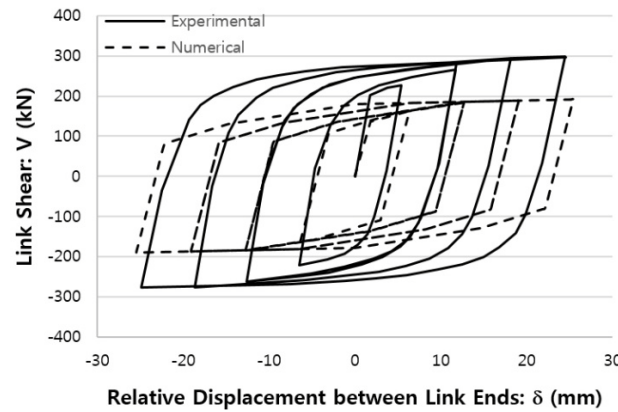
Fig. 16 Comparison of experimental and analytical link shear versus relative displacement between link ends hysteresis curves for specimen 7 using the proposed model by Richards and Uang (2005)

The numerical results of specimens 5 and 7 using the proposed model by Koboevic *et al*. (2012) are compared to the experimental results in Figs. 13-14. As shown in Figs. 13-14, the maximum predicted value of link shear force is 24 and 15 percent more than the experimental value for specimens 5 and 7, respectively. The numerical results of specimens 5 and 7 using the proposed model by Richards and Uang (2005) and Figs. 15-16. As shown in Figs. 15-16, the maximum predicted value of link shear force is 26 and 36 percent less than the experimental value for specimens 5 and 7, respectively.

3.3 Case 3

Berman and Bruneau (2007) tested a large scale single story EBF. To avoid lateral torsional buckling a tubular link was used. The test setup and the OpenSees model are shown in Fig. 17 and Fig. 18, respectively. As shown, a hydraulic actuator applied horizontal force to a loading beam that equally distributed the load to clevises at the top of each column (a small variation in the load to each column is expected due to the axial flexibility of the loading beam). The frame was mounted on clevises at the base of each column that were fastened to a foundation beam that attached to a strong floor and also to the reaction frame where the actuator was mounted. Excluding the loading beam and clevis heights, the actual height of the specimen from the centerline of the link beam to the centerline of the lower clevises, h, was set at 2360 mm. The steel specified for the link was A572 Gr. 50, which has a nominal yield strength of 345 MPa. the following link cross-section dimensions and length were chosen: $d = b = 150$ mm, $t_f = 16$ mm, $t_w = 8$ mm, and $e = 460$ mm. Braces were HSS $178 \times 178 \times 12.7$ and columns were W 310×143 and the beam-to-column, brace-to-column, and brace-to-beam connections were all designed to be moment resisting.

The quasi-static loading protocol used here was developed based on the guidelines presented in ATC-24-92. The cycles up to and including yielding were performed under force control. Beyond yield, the subsequent cycles were applied in displacement control using the horizontal displacement recorded at the link beam level. Table 3 gives the recorded values of maximum base shear (obtained from the actuator load cell output), V_a, the calculated values of percent drift and link rotation, γ, and the corresponding fraction of the yield displacement for each cycle imposed on the specimen.
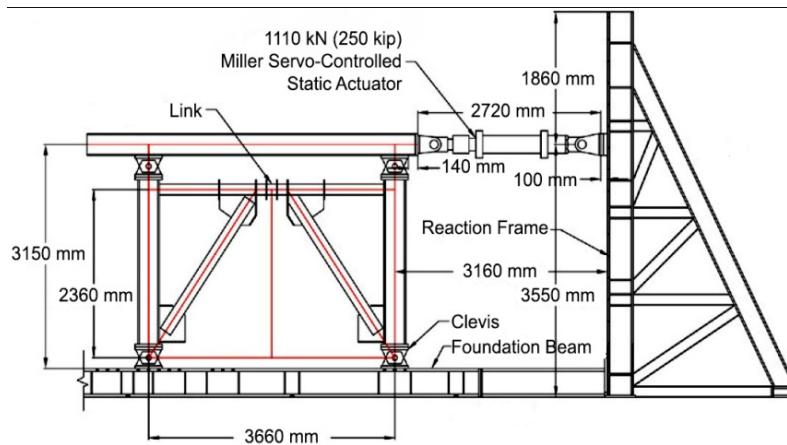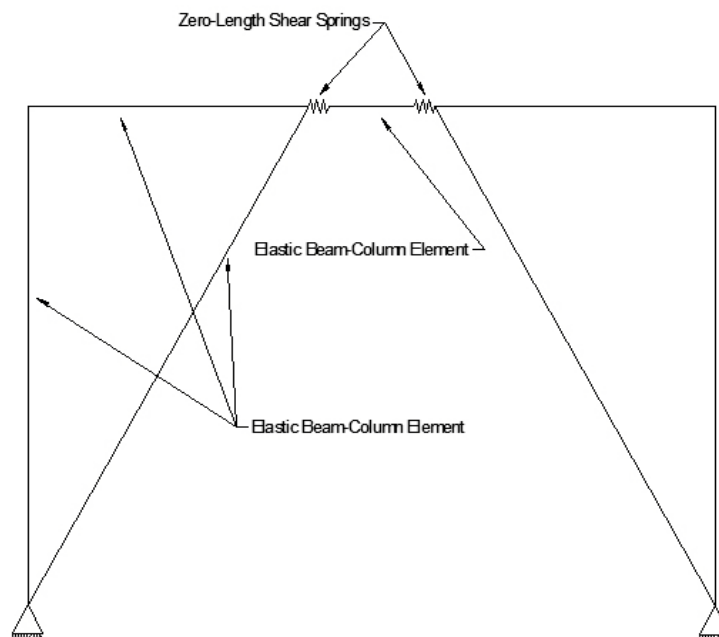
Fig. 17 Test setup (Berman and Bruneau 2007)

Fig. 18 OpenSees model for test setup

The numerical results are compared to the experimental results in Fig. 19. As shown in Fig. 19, the numerical results fit very well the experimental results and the proposed model not only predicted very well the maximum values of shear force and deformation, but also predicted very well the intermediary values. This very good fitting showed that the proposed model was able to accurately predict the inelastic response of EBF links alone and the whole EBF including link, the beams outside of the beam, braces, and columns.

The numerical results using the proposed model by Koboevic *et al*. (2012) and Richards and Uang (2005) are compared to the experimental results in Figs. 20-21, respectively. As shown in

Table 3 Loading history (Berman and Bruneau 2007)

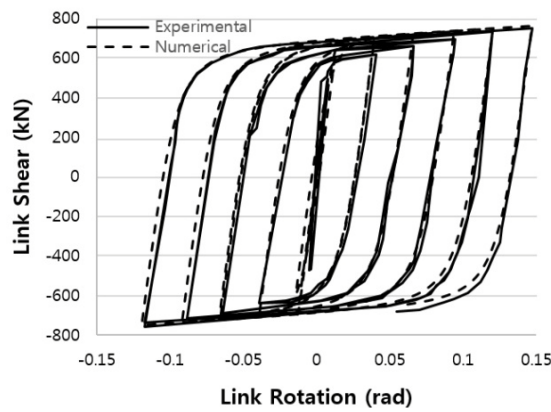| Cycle no.	Fraction of δ_y	Drift (%)	γ (rad)	V_a (kN)
1	0.33	0.11	0.004	213
2	0.33	0.11	0.004	217
3	0.33	0.11	0.004	212
4	0.67	0.23	0.008	434
5	0.67	0.23	0.008	432
6	0.67	0.24	0.009	445
7	1.0	0.38	0.014	668
8	1.0	0.37	0.013	646
9	1.0	0.37	0.013	664
10	2.0	0.76	0.038	842
11	2.0	0.75	0.037	850
12	2.0	0.75	0.037	853
13	3.0	1.15	0.067	893
14	3.0	1.14	0.066	912
15	3.0	1.14	0.066	912
16	4.0	1.54	0.096	947
17	4.0	1.52	0.093	956
18	5.0	1.92	0.123	991
19	5.0	1.92	0.123	996
20	6.0	2.30	0.151	1009

Fig. 19 Comparison of experimental and analytical link shear versus link rotation hysteresis
curves using the proposed model

Figs. 20-21 the maximum predicted value of link shear force using the proposed model by
Koboevic *et al*. (2012) and Richards and Uang (2005) is 23 and 5 percent more than the
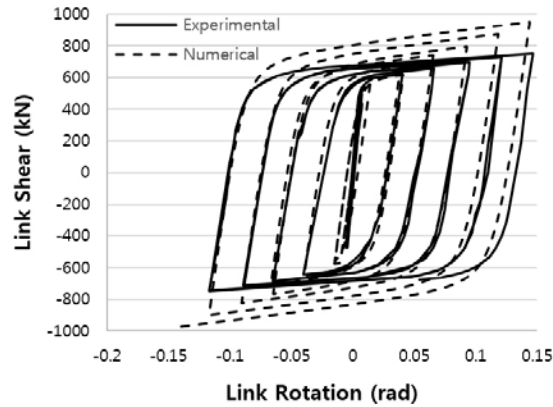experimental value, respectively.

Fig. 20 Comparison of experimental and analytical link shear versus link rotation hysteresis
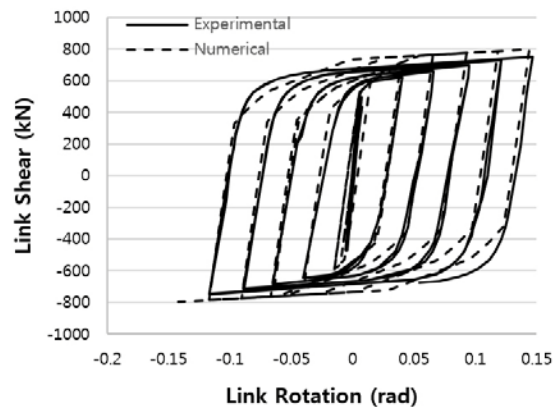curves using the proposed model by Koboevic *et al*. (2012)

Fig. 21 Comparison of experimental and analytical link shear versus link rotation hysteresis curves
using the proposed model by Richards and Uang (2005)

4. Comparison of proposed and available analytical models

To compare the numerical results of the available analytical models and the proposed analytical model, nonlinear dynamic analysis of a four-story EBF subjected to El Centro earthquake was performed. The record was scaled to a peak ground acceleration of 0.5 g. The sections of the members and dimensions of the EBF are summarized in Fig. 22. All of the connections and supports are assumed to be rigid, except the connections between bracings and the other elements, which are assumed to have a pin connection. The damping ratio was set to 5%. The maximum inelastic rotation in links was set to 0.08 radian by using the MinMax material. The main analytical results of the three analytical models are compared in Fig. 23. As shown in Fig. 23 the numerical results using the proposed analytical models by Koboevic *et al*. (2012) and Richards and Uang (2005) are close to each other. The maximum lateral displacement, the maximum brace force, the maximum link shear ratio and the maximum link moment ratio obtained from the proposed analytical model are more than those obtained from the two other analytical models.
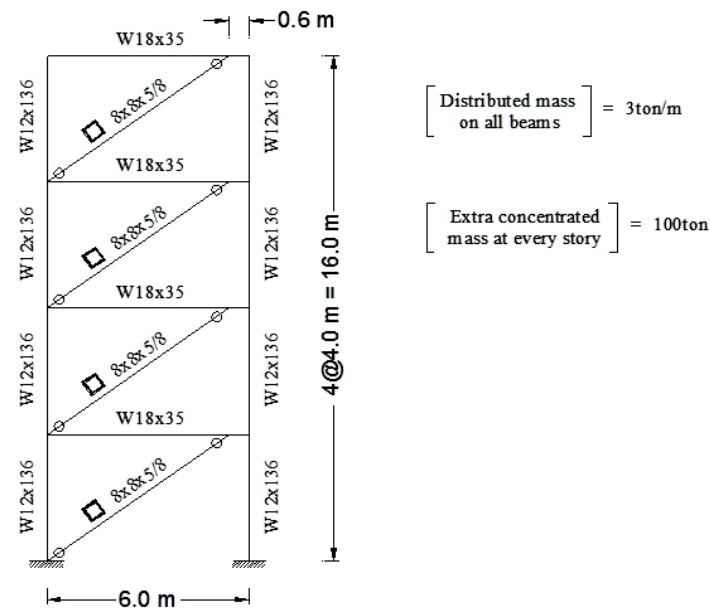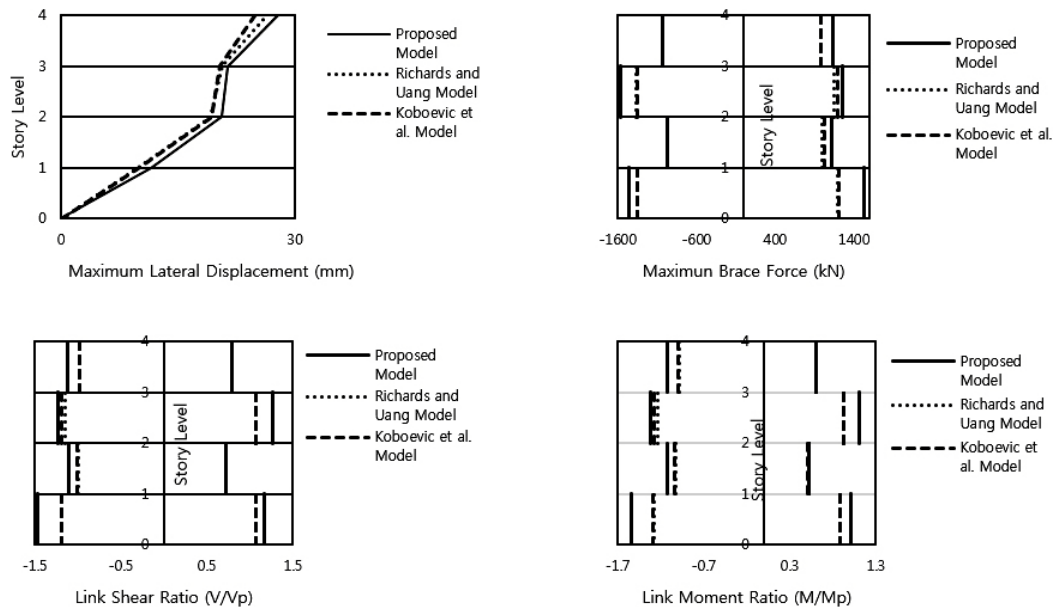
Fig. 22 Configuration of the four-story EBF

Fig. 23 Comparison of the results among the three models for the four-story EBF

5. Conclusions

It is said in the literature that available analytical models for shear links generally predict very well the maximum shear forces and deformations from experiments on shear links, but may underestimate the intermediary values. In this study it is shown that available analytical models do

not predict very well the maximum shear forces and deformations too. Koboevic *et al*. (2012) proposed an analytical model based on the results of experimental test performed by Okazaki and Engelhardt (2007), regardless of the fact that the actual measured dimensions of sections were different from the standard dimensions of sections. To account for this difference between the actual and standard dimensions of sections, despite of what is said in their paper, the strain-hardening ratio is set to 0.0045. For this reason, the shear stiffness of their proposed model is incorrect and the predicted shear forces are 15 to 24 percent more than the experimental shear forces. In this study an analytical model which can accurately predict both maximum and intermediary values of shear force and deformation was proposed. The OpenSees program is used to construct numerical models. The inelastic behavior of the shear springs was described using Giuffré-Menegotto-Pinto (Steel02) hysteretic material. The model parameters were determined by calibration against data from 11 cyclic tests on shear links by Okazaki and Engelhardt (2007). Then the proposed model is verified by comparing the predicted shear forces and deformations with the test results of 7 cyclic tests on shear links by Kasai and Popov (1986) and 1 cyclic test on a large scale 1-story EBF by Berman and Bruneau (2007). Comparison of available test results with the hysteresis curves obtained using the proposed analytical model established the accuracy of the model. To compare the numerical results of the available analytical models and the proposed analytical model, nonlinear dynamic analysis of a four-story EBF subjected to El Centro earthquake was performed. The proposed model is recommended to be used to perform inelastic analyses of EBFs.

References

AISC 341 (2010), Seismic provisions for structural steel buildings, American Institute of Steel Construction; Chicago, IL, USA.

Berman, J.W. and Bruneau, M. (2007), "Experimental and analytical investigation of tubular links for eccentrically braced frames", *Eng. Struct*., **29**(8), 1929-1938.

Daneshmand, A. and Hosseini Hashemi, B. (2012), "Performance of intermediate and long links in eccentrically braced frames", *J. Construct. Steel Res*., **70**, 167-176.

Ibarra, L.F. and Krawinkler, H. (2005), "Global collapse of frame structures under seismic excitations", Report No. 152; The John A. Blume Earthquake Engineering Center, Department of Civil and Environmental Engineering, Stanford University, CA, USA.

Kanvinde, A.M., Marshall, K.S., Grilli, D.A. and Bomba, G. (2014), "Forensic analysis of link fractures in eccentrically braced frames during the February 2011 Christchurch Earthquake: Testing and simulation", *J. Struct. Eng*., **141**(5), 04014146.

Kasai, K. and Popov, E.P. (1986), "General behavior of WF steel shear link beams", *J. Struct. Eng*., **112**(2), 362-282.

Koboevic, S., Rozon, J. and Tremblay, R. (2012), "Seismic performance of low-to-moderate height eccentrically braced steel frames designed for North American seismic conditions", *J. Struct. Eng*., **138**(12), 1465-1476.

Lian, M., Su, M. and Guo, Y. (2015), "Seismic performance of eccentrically braced frames with high strength steel combination", *Steel Compos. Struct., Int. J*., **18**(6), 1517-1539.

Montuori, R., Nastri, E. and Piluso, V. (2015), "Seismic response of EB-frames with inverted Y-scheme: TPMC versus eurocode provisions", *Earthq. Struct., Int. J*., **8**(5), 1191-1214.

Okazaki, T. and Engelhardt, M.D. (2007), "Cyclic loading behavior of EBF links constructed of ASTM A992 steel", *J. Construct. Steel Res*., **63**(6), 751-765.

Ohsaki, M. and Nakajima, T. (2012), "Optimization of link member of eccentrically braced frames for maximum energy dissipation", *J. Construct. Steel Res*., **75**, 38-44.

Okazaki, T., Engelhardt, M.D., Hong, J.K., Uang, C.M. and Drolias, A. (2014), "Improved link-to-column connections for steel eccentrically braced frames", *J. Struct. Eng*., **141**(8), 04014201.

O'Reilly, G.J. and Sullivan, T.J. (2013), "Direct displacement-based seismic design of steel eccentrically braced frame structures", *Bull. Earthq. Eng*., **11**(6), 2197-2231.

O'Reilly, G.J. and Sullivan, T.J. (2016), "Fragility functions for eccentrically braced steel frame structures", *Earthq. Struct., Int. J*., **10**(2), 367-388.

Ramadan, T. and Ghobarah, A. (1995), "Analytical model for shear-link behavior", *J. Struct. Eng*., **121**(11), 1574-1580.

Richards, P.W. and Uang, C.M. (2005), "Effect of flange width-thickness ratio on eccentrically braced frames link cyclic rotation capacity", *J. Struct. Eng*., **131**(10), 1546-1552.

Richards, P.W. and Uang, C.M. (2006), "Testing protocol for short links in eccentrically braced frames", *J. Struct. Eng*., **132**(8), 1183-1191.

Ricles, J.M. and Popov, E.P. (1994), "Inelastic link element for EBF seismic analysis", *J. Struct. Eng*., **120**(2), 441-463.

Wang, F., Su, M., Hong, M., Guo, Y. and Li, S. (2016), "Cyclic behaviour of Y-shaped eccentrically braced frames fabricated with high-strength steel composite", *J. Construct. Steel Res*., **120**, 176-187.

Xu, X., Zhang, Y. and Lou, Y. (2016), "Self-centering eccentrically braced frames using shape memory alloy bolts and post-tensioned tendons", *J. Construct. Steel Res*., **125**, 190-204.

CC